Proceedings of the 25th International Conference on
**Port and Ocean Engineering under Arctic Conditions**
June 9-13, 2019, Delft, The Netherlands

# A study of the transition ice speed from intermittent crushing to frequency lock-in vibrations based on model-scale experiments

Cody C. Owen[1], Hayo Hendrikse[1]
[1] Delft University of Technology, Delft, the Netherlands

## ABSTRACT

For the design of offshore structures in regions with ice-infested waters, the prediction of interaction between ice floe and support structure is essential. If the structure is vertically sided at the ice-structure interface, then ice-induced vibrations can develop. Recently, a dynamic ice-structure interaction model has been developed and validation has been attempted based on dedicated experiments. This study extends the validation by investigating the capabilities of the analytical model in predicting the indentation speed at which transition from the intermittent crushing to frequency lock-in regime of ice-induced vibrations occurs with various input parameters. Implementation of these various input parameters seeks to address the challenge of adapting the analytical model from the reference input parameters to scenarios with other structural properties. Using these various input parameters, the analytical model can demonstrate accurate prediction of the transition ice speed from intermittent crushing to frequency lock-in vibrations as observed in the experiments when the mean global ice load in crushing is properly estimated. For the cases when the mean global ice load was not properly estimated, either unsuitable scaling between input parameters, undesirable behavior of the model ice during the experiments, or a combination thereof may be the cause. Overall, this study serves to establish the range of applicability for the analytical model in terms of accurate prediction of intermittent crushing and frequency lock-in vibrations between model ice and various structures. In addition, this study provides general trends about the effect of change of structural properties and initial conditions on the transition ice speed from intermittent crushing to frequency lock-in vibrations.

KEY WORDS: Ice-induced vibrations; model ice; structural shape; validation.

## INTRODUCTION

For the design of offshore structures in regions with ice-infested waters, the prediction of interaction between ice floe and support structure is essential. If the structure is sufficiently flexible and vertically sided at the ice-structure interface, and the ice is sufficiently strong and thick, then ice-induced vibrations can develop. Some ice-structure interaction models have attempted to predict ice-induced vibrations, but issues have arisen regarding their range of applicability for various dynamic properties of the structures (Jeong and Baddour, 2010; Kärnä et al., 2013; Muhonen, 1996). Recently, a phenomenological model has been developed and validation has been attempted based on dedicated experiments (Hendrikse et al., 2018). These experiments belong to an extensive model-scale testing campaign as part of the Ice-induced Vibrations of Offshore Structures (IVOS) project and were conducted by the Hamburg Ship Model Basin (HSVA); a summary is provided by Ziemer (2017). From the validation attempt of the analytical model, input parameters to define the model ice behavior were derived with a reference structure. With the previously determined input parameters, experiments from the IVOS project with similar ice conditions but with structures that differ from the reference structure were simulated to investigate the capabilities of the analytical model.

The first part of the investigation demonstrated that the model can accurately predict the indentation speed range of frequency lock-in vibrations for various structural configurations, provided that the mean global ice load in crushing is properly estimated (Owen and Hendrikse, 2018). This study expands the investigation to show that the model can accurately predict the development of intermittent crushing vibrations as experimentally observed and the indentation speed at which transition from intermittent crushing to frequency lock-in vibrations occurs, and to assess the effect of change of structural properties on that transition. The working principle is that if the mean global ice load is properly estimated in the analytical model, then the intermittent crushing, frequency lock-in, and continuous brittle crushing regimes of ice-induced vibrations should be correctly predicted irrespective of the structural properties. Determining an accurate global ice load level is dependent on the scaling from the predetermined reference parameters to other parameters. In this study, it is proven that proper estimation of the global ice load by the analytical model can produce results that correspond well with experimental observations in the three regimes of ice-induced vibrations, in addition to predicting the transitions from intermittent crushing to frequency lock-in to continuous brittle crushing vibrations. Furthermore, the effect of change of structural properties, as well as initial conditions, on the transition ice speed from intermittent crushing to frequency lock-in vibrations is assessed. This is a first step towards a formula that can estimate the transition ice speeds for the purpose of structural design.

## IVOS EXPERIMENTAL CAMPAIGN

The Phase 3 experiments of the IVOS campaign with model ice were conducted in 2018 by HSVA in their Large Ice Basin (Ziemer, 2018). During the campaign, model structures with various configurations of size, cross-sectional geometry (shape) at the ice-structure interface, fundamental natural frequency, and stiffness were utilized for indentation tests in model ice over a range of indentation speeds (Ziemer and Hinse, 2017). Figure 1 illustrates the test apparatus and size and shape of the model structures of the IVOS experiments that are

specifically chosen for this study. Detailed ice properties were recorded for each of the experiments and the pertinent measurements, and their use, are elaborated in a later section.

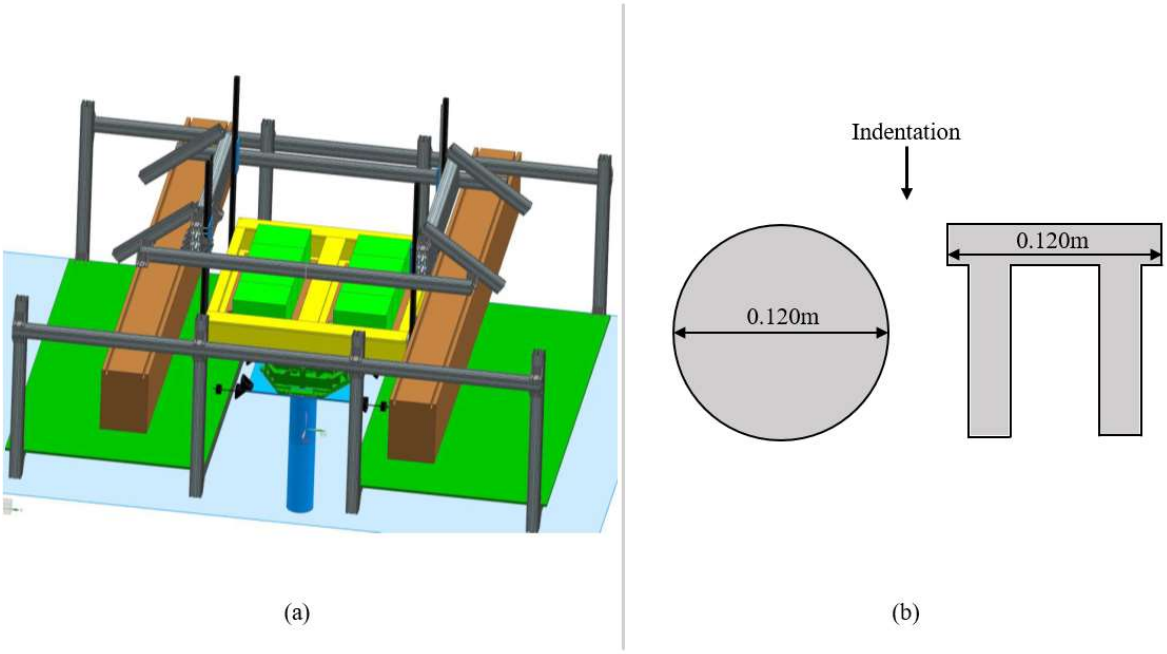


Figure 1. Schematics of the test apparatus and size and shape of select model structures from the IVOS experiments, of which (a) is the Phase 3 test apparatus; and (b) is the schematic of model structure cross-sections with shape, size, and orientation of indentation (Hinse et al., 2017; Ziemer, 2018). Shown in the schematic of the test apparatus are the model structure in blue, the 6-component load cell in green above the model structure, the compliant base in yellow, added masses in light green on top of the compliant base, and the bending rods in black that connect the compliant base to the rigid girders, in brown, of the main carriage in the ice basin.

## ANALYTICAL MODEL

The analytical model used for this study is described in Hendrikse and Nord (2019). The reference parameters to define the HSVA model ice behavior have been determined in Hendrikse et al. (2018) and are shown in Table 1. The scaling approach from the reference input parameters to other parameters, such as structural size and shape, is discussed in Owen and Hendrikse (2018).

Table 1. Reference input parameters from HSVA model ice for the analytical model derived from the indentation experiment with the rigid reference structure of 0.2 m width and 1150 N mean brittle crushing load (Hendrikse et al., 2018).

| $K_{2,ref}$ [N m$^{-1}$] | $C_{2,ref}$ [N$^3$ m$^{-1}$ s] | $K_{1,ref}$ [N m$^{-1}$] | $C_{1,ref}$ [N m$^{-1}$ s] | $N_{ref}$ [-] | $r_{max,ref}$ [m] | $\delta_{f,ref}$ [m] |
|---|---|---|---|---|---|---|
| $5.091 \cdot 10^4$ | $1.05 \cdot 10^9$ | $5.372 \cdot 10^3$ | $1.7021 \cdot 10^4$ | 39 | $2.9 \cdot 10^{-3}$ | $2 \cdot 10^{-3}$ |

## SIMULATION PARAMETERS

The input parameters to the analytical model for the simulations are shown in Table 2. Each structure is simulated as a single-degree-of-freedom (SDOF) oscillator, which follows the design objective of the test apparatus from the IVOS experiments. The structural shape and the corresponding shape factor, $s_s(s,s_{ref})$, are provided in Table 2 and explained in Owen and Hendrikse (2018). The structural width $d$, fundamental natural frequency $f_s$, and stiffness $K_s$ of each model structure were provided by HSVA (Ziemer, 2018). The damping as a ratio of critical damping $\zeta_s$ was determined by logarithmic decrement from a relaxation test for each of the structures (Owen, 2017). It was observed during the experiments that the properties of the model ice varied spatially throughout the basin and among the different ice sheets. To capture effects of the variation of ice properties on the ice-structure interaction, a range of ice thickness $h$ and uniaxial compressive strength $\sigma$ are considered for the simulations. Each structure, therefore, is subjected to a set of two different ice condition cases in the simulations. The first case includes the minimum ice thickness and minimum compressive strength as determined from the corresponding experiments. The second case includes the maximum ice thickness and maximum compressive strength.

The mean load adjustment factor $f_\mu$ is determined a posteriori as the ratio of the experimental and simulated mean global ice load in crushing for the highest tested indentation speed. This factor is applied in a similar manner as the shape factor, is used to examine the effect of proper estimation of mean global ice load in crushing on the development of the three regimes of ice-induced vibrations, and is used in trials T23 and T33 for comparison with the corresponding baseline simulations of T22 and T32, respectively. The initial displacement $u_{s,0}$ and velocity $\dot{u}_{s,0}$ of the structure are set to zero for the baseline simulations (the first eight trials) and are non-zero in the final eight trials (T53 to T60) in order to investigate the effect of initial conditions on the development of the indentation speed ranges of the three ice-induced vibrations regimes. The trials T41 to T52 are conducted to study the effect of the change in structural properties on the transition speed from intermittent crushing to frequency lock-in vibrations. The baseline trials for the structural property change study are T01 and T02. The structural property study includes the following: decrease (T41, T42) and increase (T43, T44) in damping as a fraction of critical damping $\zeta_s$; decrease (T45, T46) and increase (T47, T48) in natural frequency $\omega_n$; and decrease (T49, T50) and increase (T51, T52) in structural mass $M_s$.

For each trial, simulations are performed from an indentation speed of 0.005 m $s^{-1}$ to 0.200 m $s^{-1}$ with increments of 0.005 m $s^{-1}$ as performed in the experiments. Each simulation is executed for 40 seconds and the final 20 seconds are exclusively considered for analysis of the steady-state response.

## BASELINE COMPARISON OF EXPERIMENTS AND SIMULATIONS

To compare the experiments and simulations regarding the three distinct regimes of ice-induced vibrations, criteria are defined to identify each particular regime. Beginning at lower indentation speeds, intermittent crushing vibrations can be categorized based on structural displacement and global ice load time histories following a sawtooth-like pattern (see Hendrikse and Nord (2019) for a summary of observations). Additionally, approximately two frequencies should be present in the structural response: the transient of the structure succeeding the cascading failure of the ice after maximum global ice load, and the frequency associated with the sawtooth-like

load build-up prior to the cascading failure of the ice. Relatively, the maximum global ice loads during intermittent crushing vibrations should be greater than or equal to those observed during frequency lock-in vibrations. Some leniency was applied when selecting the experimental observations of intermittent crushing vibrations, specifically regarding the exact predicted frequencies and magnitude of global ice loads.

Table 2. Input parameters to the analytical model for simulation of the IVOS experiments.

| Trial name | Shape | $s_s(s,s_{ref})$ [-] | $d$ [m] | $f_s$ [Hz] | $K_s$ [kN m$^{-1}$] | $\zeta_s$ [%] | $h$ [m] | $\sigma$ [kPa] | $f_\mu$ [-] | $u_{s,0}$ [m] | $\dot{u}_{s,0}$ [m s$^{-1}$] |
|---|---|---|---|---|---|---|---|---|---|---|---|
| T01 | ■ | 1.0 | 0.120 | 2.15 | 378 | 1.9 | 0.039 | 110 | 1 | 0 | 0 |
| T02 | ■ | 1.0 | 0.120 | 2.15 | 378 | 1.9 | 0.054 | 154 | 1 | 0 | 0 |
| T11 | ■ | 1.0 | 0.120 | 5.18 | 1910 | 1.8 | 0.039 | 110 | 1 | 0 | 0 |
| T12 | ■ | 1.0 | 0.120 | 5.18 | 1910 | 1.8 | 0.054 | 154 | 1 | 0 | 0 |
| T21 | ■ | 1.0 | 0.120 | 5.18 | 1910 | 1.8 | 0.058 | 109 | 1 | 0 | 0 |
| T22 | ■ | 1.0 | 0.120 | 5.18 | 1910 | 1.8 | 0.088 | 212 | 1 | 0 | 0 |
| T31 | ● | 0.8 | 0.120 | 5.18 | 1910 | 1.8 | 0.058 | 109 | 1 | 0 | 0 |
| T32 | ● | 0.8 | 0.120 | 5.18 | 1910 | 1.8 | 0.088 | 212 | 1 | 0 | 0 |
| T23 | ■ | 1.0 | 0.120 | 5.18 | 1910 | 1.8 | 0.088 | 212 | **1.9** | 0 | 0 |
| T33 | ● | 0.8 | 0.120 | 5.18 | 1910 | 1.8 | 0.088 | 212 | **1.9** | 0 | 0 |
| T41 | ■ | 1.0 | 0.120 | 2.15 | 378 | **1.9/5** | 0.039 | 110 | 1 | 0 | 0 |
| T42 | ■ | 1.0 | 0.120 | 2.15 | 378 | **1.9/5** | 0.054 | 154 | 1 | 0 | 0 |
| T43 | ■ | 1.0 | 0.120 | 2.15 | 378 | **1.9·5** | 0.039 | 110 | 1 | 0 | 0 |
| T44 | ■ | 1.0 | 0.120 | 2.15 | 378 | **1.9·5** | 0.054 | 154 | 1 | 0 | 0 |
| T45 | ■ | 1.0 | 0.120 | **2.15/√5** | **378/5** | 1.9 | 0.039 | 110 | 1 | 0 | 0 |
| T46 | ■ | 1.0 | 0.120 | **2.15/√5** | **378/5** | 1.9 | 0.054 | 154 | 1 | 0 | 0 |
| T47 | ■ | 1.0 | 0.120 | **2.15·√5** | **378·5** | 1.9 | 0.039 | 110 | 1 | 0 | 0 |
| T48 | ■ | 1.0 | 0.120 | **2.15·√5** | **378·5** | 1.9 | 0.054 | 154 | 1 | 0 | 0 |
| T49 | ■ | 1.0 | 0.120 | 2.15 | **378/5** | 1.9 | 0.039 | 110 | 1 | 0 | 0 |
| T50 | ■ | 1.0 | 0.120 | 2.15 | **378/5** | 1.9 | 0.054 | 154 | 1 | 0 | 0 |
| T51 | ■ | 1.0 | 0.120 | 2.15 | **378·5** | 1.9 | 0.039 | 110 | 1 | 0 | 0 |
| T52 | ■ | 1.0 | 0.120 | 2.15 | **378·5** | 1.9 | 0.054 | 154 | 1 | 0 | 0 |
| T53 | ■ | 1.0 | 0.120 | 2.15 | 378 | 1.9 | 0.039 | 110 | 1 | **0.01** | 0 |
| T54 | ■ | 1.0 | 0.120 | 2.15 | 378 | 1.9 | 0.054 | 154 | 1 | **0.01** | 0 |
| T55 | ■ | 1.0 | 0.120 | 5.18 | 1910 | 1.8 | 0.039 | 110 | 1 | **0.01** | 0 |
| T56 | ■ | 1.0 | 0.120 | 5.18 | 1910 | 1.8 | 0.054 | 154 | 1 | **0.01** | 0 |
| T57 | ■ | 1.0 | 0.120 | 5.18 | 1910 | 1.8 | 0.058 | 109 | 1 | **0.01** | 0 |
| T58 | ■ | 1.0 | 0.120 | 5.18 | 1910 | 1.8 | 0.088 | 212 | 1 | **0.01** | 0 |
| T59 | ● | 0.8 | 0.120 | 5.18 | 1910 | 1.8 | 0.058 | 109 | 1 | **0.01** | 0 |
| T60 | ● | 0.8 | 0.120 | 5.18 | 1910 | 1.8 | 0.088 | 212 | 1 | **0.01** | 0 |

For higher indentation speeds, the frequency lock-in regime of SDOF structures can be defined by the ratio of the maximum structural velocity and the indentation speed, known as $\beta$, between 1.0 and 1.5 (see Hendrikse and Nord (2019) for a summary of observations). Following this definition, the experiments and simulations are examined for recurring instances when $\beta$ is between 1.0 and 1.5, when the structural response is quasi-sinusoidal near the fundamental natural frequency, and when the global ice load periodically is amplified ensuing the time when the relative velocity between ice and structure is low. For this study, adequate development of frequency lock-in vibrations is achieved for the experiments when the aforementioned criteria are met for at least three consecutive cycles. The choice of at least three consecutive cycles is

made in an attempt to inclusively identify frequency lock-in vibrations as a result of nearly constant ice conditions. But because the ice conditions were known to vary substantially for a given indentation speed, requiring more consecutive cycles could potentially exclude indentation speeds during which frequency lock-in vibrations develop. The simulated results are considered frequency lock-in vibrations when the aforementioned criteria are met for a majority of the time history.

With the highest indentation speeds, the continuous brittle crushing regime can be categorized by a stochastic global ice load time history with maximum and mean global ice loads that are not greater than those observed during intermittent crushing and frequency lock-in vibrations (Hendrikse, 2017). Moreover, the structural response is similar to that of a structure excited by an aperiodic load with maximum and mean structural displacements that are lower than those observed during intermittent crushing and frequency lock-in vibrations. Finally, the $\beta$ value is less than 1.0 for any three consecutive cycles of structural vibration.

Figure 2 shows the comparison between the experimental observations of ice-induced vibrations and the simulated transition speeds from intermittent crushing (ICR) to frequency lock-in (FLI) to continuous brittle crushing (CBR) vibrations. The overlap in transition from one regime of ice-induced vibrations to another depicts the variation in the transition as a result of the range of ice conditions simulated. Overall, the predicted transition speeds from intermittent crushing to frequency lock-in to continuous brittle crushing vibrations are in close agreement with the experimental observations. In the trial set of T31 and T32 (denoted T31&32), the transition speeds from intermittent crushing to frequency lock-in to continuous brittle crushing vibrations are markedly underpredicted. These can be explained by an improper estimation of the mean global ice load in crushing as discussed in Owen and Hendrikse (2018). To address this issue, trials T23 and T33 (see Table 2) were executed as previously mentioned and the results are compared with the respective baseline trials in Figure 3. Since the simulated mean global ice load in crushing was underestimated by the scaling approach for the trials of T22 and T32, the factor $f_\mu$ was applied for the maximum ice conditions to extend the upper bounds of the transition speeds from intermittent crushing to frequency lock-in to continuous brittle crushing vibrations. It can be seen in Figure 3 that the simulated results capture better the transition speeds as experimentally observed, albeit with greater overlap.

Exemplary simulated and experimentally observed time histories of intermittent crushing and frequency lock-in vibrations are shown in Figure 4 and Figure 5, respectively. A low-pass filter with cutoff frequency of 49 Hz was applied to the experimental global ice load and structural response signals to attenuate noise from the data acquisition power source, and was applied to the simulated ice load and structural response signals for comparative consistency. In Figure 4, the comparison between the experimental and simulated time histories is adequate considering that the analytical model only includes a SDOF oscillator. During intermittent crushing vibrations, higher modes of the test apparatus are likely excited and dissipation of energy from the ice-structure interaction via the higher modes occurs more quickly, the effect of which cannot be captured by the SDOF oscillator; this results in the difference in transient structural response between the experimental and simulated time histories.

## SENSITIVITY TO STRUCTURAL PROPERTIES AND INITIAL CONDITIONS

The effect of the change of structural properties of an SDOF oscillator on the transition speeds between the three regimes of ice-induced vibrations can be expressed using the following equation of motion:

$$\ddot{u}_s + 2\zeta_s\omega_n\dot{u}_s + \omega_n^2 u_s = F_{ice}(t,u_s,\dot{u}_s) \,/\, M_s \quad (1)$$

where $u_s$ is the structural displacement, the overdots represent time derivatives of the structural response, and $F_{ice}$ is the global ice-induced load on the structure. Based on this formulation of the equation of motion of the system, the three structural properties of interest are the damping ratio, the natural frequency, and the mass of the structure. Using the baseline trial set of T01 and T02, the three structural properties are individually varied with respect to the baseline and simulations are run as previously mentioned (T41 to T52) and the results are presented in Figure 6. The subsequent findings agree with those stated in Hendrikse (2017) regarding the effect of changes in structural properties on the prediction of development of frequency lock-in vibrations. For a decrease in the damping ratio, the transition speed from frequency lock-in to continuous brittle crushing vibrations increases and the overlap increases. The transition speed from intermittent crushing to frequency lock-in vibrations remains roughly the same. For an increase in the damping ratio, the transition speed from frequency lock-in to continuous brittle crushing vibrations decreases and the overlap decreases. The transition speed from intermittent crushing to frequency lock-in vibrations decreases, but less significantly than the other transition speed. For a decrease in the natural frequency, the transition speed from intermittent crushing to frequency lock-in vibrations increases and the overlap increases. The transition speed from frequency lock-in to continuous brittle crushing vibrations increases but with similar overlap, and with slightly less increase than the other transition speed. For an increase in the natural frequency, the transition speed from intermittent crushing to frequency lock-in vibrations decreases and the overlap decreases. The transition speed from frequency lock-in to continuous brittle crushing vibrations decreases and the overlap decreases, and with slightly more decrease than the other transition speed. Finally, for a decrease in the structural mass, the transition speed from intermittent crushing to frequency lock-in vibrations increases and the overlap increases. The transition speed from frequency lock-in to continuous brittle crushing vibrations increases with roughly the same increase as the other transition speed and the overlap decreases. For an increase in the structural mass, the transition speed from intermittent crushing to frequency lock-in vibrations decreases and the overlap decreases. The transition speed from frequency lock-in to continuous brittle crushing vibrations decreases with slightly more decrease than the other transition speed and the overlap decreases. The general trends are summarized in Table 3.

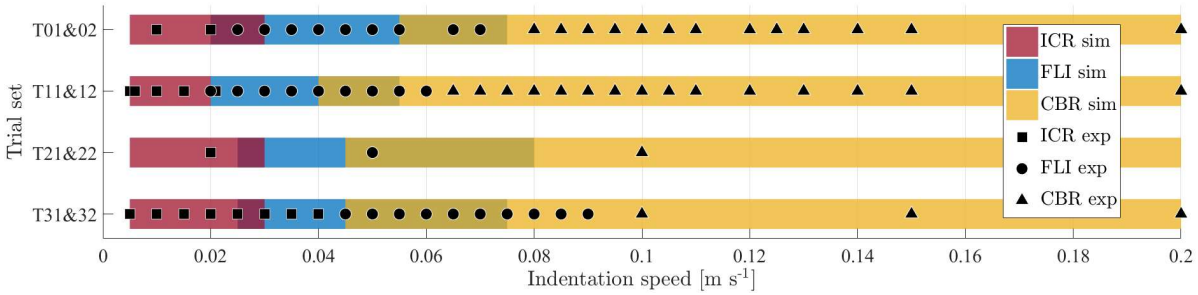


Figure 2. Baseline comparison of the simulated (sim) ranges and experimental (exp) observations of intermittent crushing (ICR), frequency lock-in (FLI), and continuous brittle crushing (CBR) regimes of ice-induced vibrations. The simulated ranges indicate the indentation speeds during which the different regimes of ice-induced vibrations develop for the range of ice conditions.

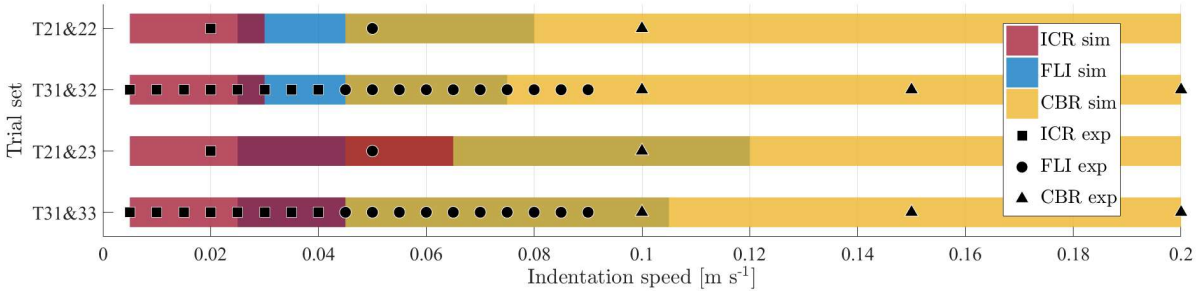


Figure 3. Comparison of the simulated (sim) ranges and experimental (exp) observations of intermittent crushing (ICR), frequency lock-in (FLI), and continuous brittle crushing (CBR) regimes of ice-induced vibrations with mean load adjustments for the relevant trial sets. The simulated ranges indicate the indentation speeds during which the different regimes of ice-induced vibrations develop for the range of ice conditions.

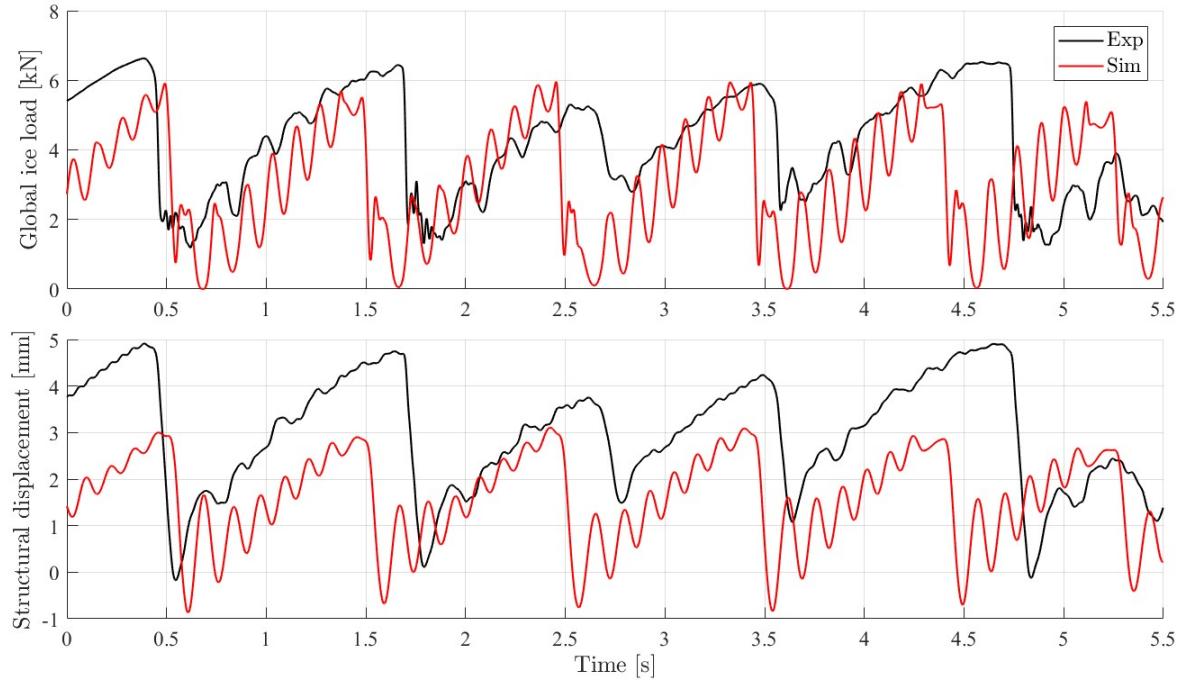


Figure 4. Comparison of global ice load and structural displacement time histories in the intermittent crushing regime from experimental (Exp) results and simulated (Sim) results with maximum ice conditions (trial T32) at an indentation speed of 0.010 m $s^{-1}$.

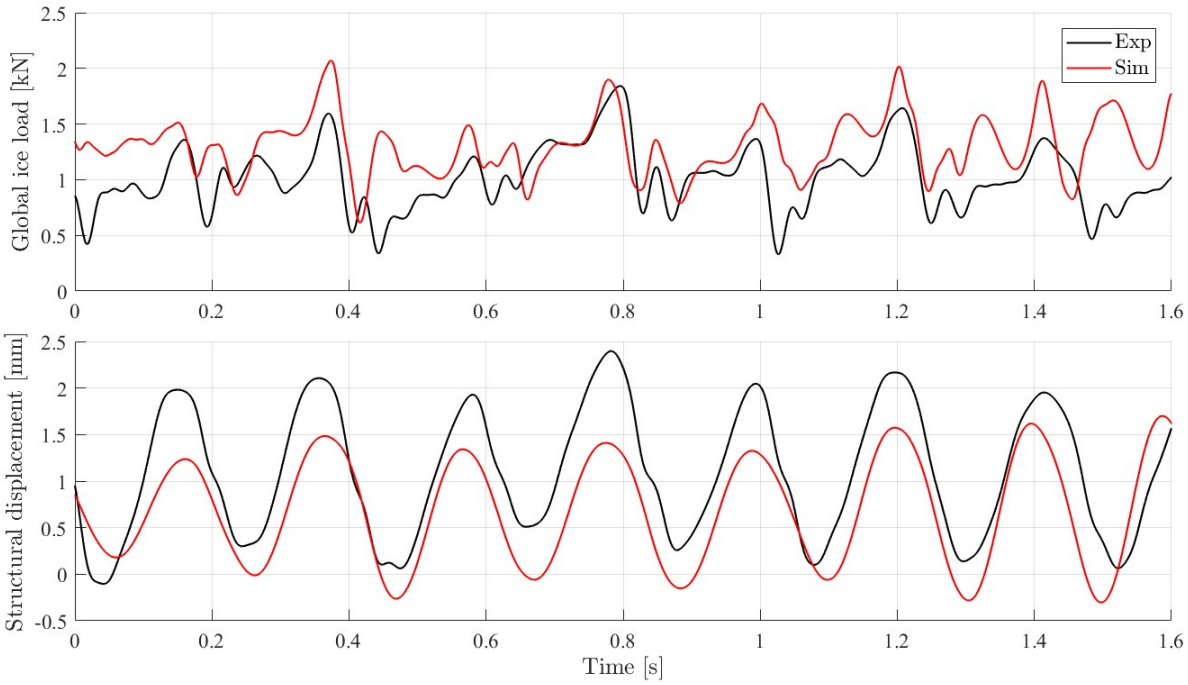


Figure 5. Comparison of global ice load and structural displacement time histories in the frequency lock-in regime from experimental (Exp) results and simulated (Sim) results with maximum ice conditions (trial T12) at an indentation speed of 0.025 m $s^{-1}$.

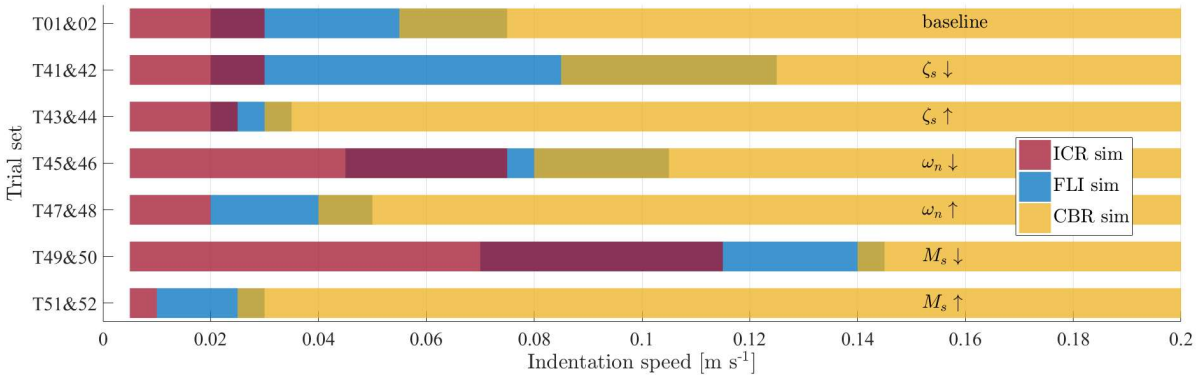


Figure 6. Results on the effect of change of structural properties on the transition speeds between the ice-induced vibrations regimes for the baseline trial set of T01 and T02.

Table 3. Recapitulation of the effect of individual changes in structural properties on the indentation speed ranges during which frequency lock-in vibrations develop and the transition ice speeds between the three regimes of ice-induced vibrations. Down- and up- arrows indicate property decreases and increases, respectively. Hyphens indicate negligible or no change.

| $\zeta_s$ | $\omega_n$ | $M_s$ | ICR-FLI overlap | FLI lower bound | FLI upper bound | FLI-CBR overlap |
|---|---|---|---|---|---|---|
| ↓ | - | - | - | - | ↑ | ↑ |
| ↑ | - | - | ↓ | - | ↓ | ↓ |
| - | ↓ | - | ↑ | ↑ | ↑ | ↑ |
| - | ↑ | - | ↓ | - | ↓ | ↓ |
| - | - | ↓ | ↑ | ↑ | ↑ | ↓ |
| - | - | ↑ | ↓ | ↓ | ↓ | ↓ |

To assess the effect of initial conditions on the transition speeds from intermittent crushing to frequency lock-in to continuous brittle crushing vibrations, the trials of T53 to T60 were conducted. For each of these trials, a large initial displacement was introduced to the structural model and the results are illustrated in Figure 7. Generally, the initial displacement affected the steady-state response of the frequency lock-in regime by increasing the upper bound of the development of frequency lock-in vibrations. Moreover, the transition speed from frequency lock-in to continuous brittle crushing vibrations tended to increase and with increased overlap. The transition speed from intermittent crushing to frequency lock-in vibrations remained roughly the same, although with some propensity to increase but less significantly than the other transition speed. The overlap for this transition speed remained roughly the same.

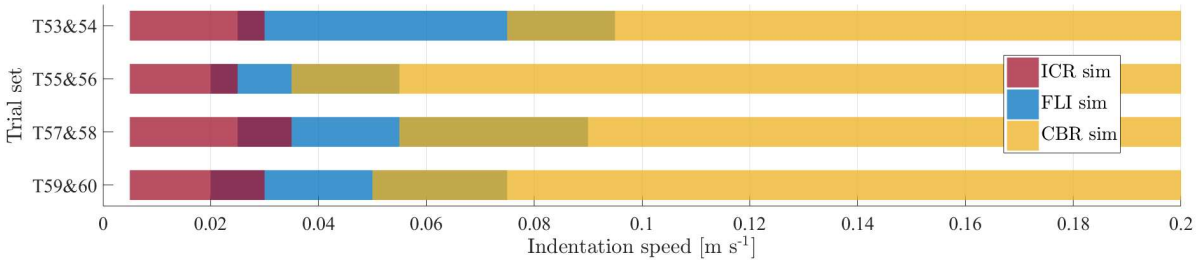


Figure 7. Results on the effect of initial conditions on the transition speeds between the ice-induced vibrations regimes for the baseline trial sets.

## DISCUSSION

Based on the general trends from the experiments, the analytical model can demonstrate accurate prediction of the transition ice speeds from intermittent crushing to frequency lock-in vibrations. Furthermore, the analytical model can show accurate prediction of the transition speeds from frequency lock-in to continuous brittle crushing vibrations. However, these accurate predictions are predicated on proper estimation of the mean global ice load level by the analytical model. As deduced in Owen and Hendrikse (2018), the type of scaling implemented may not be suitable for the input parameters that differ significantly from the reference parameters. But because the model ice in Phase 3 was effectually prepared to minimize flexural behavior, i.e. the model ice failed primarily in crushing, the unsuitable scaling of the input parameters is the most likely cause for the improper estimation of the mean global ice load in crushing.

As described in the previous section, individual changes in natural frequency, mass, and damping ratio of the structure strongly influence the predictions made by the analytical model of the transition ice speeds from intermittent crushing to frequency lock-in to continuous brittle crushing vibrations. For example, an increase in the natural frequency of the structure causes a decrease in the range of indentation speeds during which frequency lock-in vibrations develop by shifting the upper bound to a lower indentation speed. This trend was also observed by Huang et al. (2007) during analogous model-scale indentation experiments in urea ice. A decrease in the damping ratio causes little to no change in the transition ice speed from intermittent crushing to frequency lock-in vibrations, whereas a decrease in natural frequency or structural mass yields an increase in the transition ice speed from intermittent crushing to frequency lock-in vibrations. However, for a decrease in either of the three structural properties,

the transition ice speed from frequency lock-in to continuous brittle crushing vibrations increases. Note that with amply high structural mass or natural frequency, or even damping ratio, the ice-structure interaction with a rigid structure is recovered such that negligible interaction occurs (see Hendrikse and Nord (2019) for more information).

Generally, an initial displacement of the structure tended to extend the upper bound of development of frequency lock-in vibrations to higher indentation speeds, and moved the transition from frequency lock-in to continuous brittle crushing vibrations to higher indentation speeds. But the initial displacement had little to no noticeable effect on the transition ice speed from intermittent crushing to frequency lock-in vibrations.

As a general guide, and to some extent, an individual increase in natural frequency, mass, or damping ratio of the structure decreases the range of indentation speeds during which intermittent crushing and frequency lock-in vibrations develop and may shift the upper bounds of both regimes to lower indentation speeds. Conversely, an individual decrease in natural frequency, mass, or damping ratio of the structure increases the range of indentation speeds during which intermittent crushing and frequency lock-in vibrations develop and may shift the upper bounds of both regimes to higher indentation speeds. Attempts have been made with limited success to derive an equation to predict the development of the three regimes of ice-induced vibrations, as well as the transition ice speeds between these regimes (Kärnä et al., 2007; Yap and Palmer, 2013; Ziemer and Hinse, 2017). Although no closed-form solution is offered in this study, the general trends provided should be recoverable by any applicable formula and therefore can be established as a basis for further investigation.

In terms of indentation speed, it is observed that the transition from intermittent crushing to frequency lock-in vibrations is gradual, whereas the transition from frequency lock-in to continuous brittle crushing vibrations is typically abrupt and drastic. This is most apparent in the comparison of maximum structural velocity and indentation speed (see Figure 8).

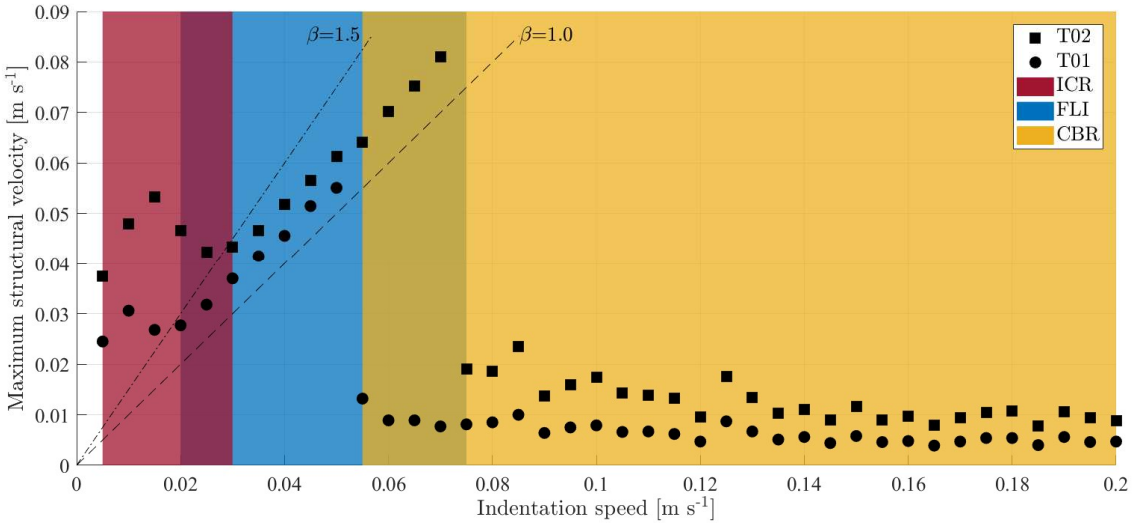


Figure 8. Example case (trial set of T01 and T02) of the difference in transition from intermittent crushing (ICR) to frequency lock-in (FLI) and from frequency lock-in to continuous brittle crushing (CBR) vibrations based on change in maximum structural velocity as a function of indentation speed.

## CONCLUSION

Experiments in model ice from Phase 3 of the IVOS project have been simulated using the analytical model with reference input parameters from a reference structure and accurate predictions of the transition ice speeds from intermittent crushing to frequency lock-in vibrations for each experiment have been shown. Furthermore, accurate predictions of the transition speeds from frequency lock-in to continuous brittle crushing vibrations for each experiment have also been presented. Proper estimation of the mean global ice load level in crushing is demonstrated to be very important for accurate prediction of the transition speeds from intermittent crushing to frequency lock-in to continuous brittle crushing vibrations, as was similarly concluded in Owen and Hendrikse (2018) for the range of indentation speeds during which frequency lock-in vibrations develop.

Individual changes in properties of the structure strongly influence the predictions made by the analytical model of the transition ice speeds from intermittent crushing to frequency lock-in to continuous brittle crushing vibrations. Typically, an individual increase in natural frequency, mass, or damping ratio of the structure decreases the range of indentation speeds during which intermittent crushing and frequency lock-in vibrations develop and shifts the upper bounds of both regimes to lower indentation speeds, and vice versa. Additionally, an initial displacement of the structure tended to extend the upper bound of development of frequency lock-in vibrations to higher indentation speeds, and moved the transition from frequency lock-in to continuous brittle crushing vibrations to higher indentation speeds. These general trends, as determined in this study, establish a foundation from which a closed-form solution may be derived by means of further investigation.

## ACKNOWLEDGEMENTS

The authors gratefully acknowledge the support from the SAMCoT CRI through the Research Council of Norway and all of the SAMCoT partners. In particular, the authors wish to thank partners involved in the IVOS project: DNV GL, Engie SA, Kvaerner AS, Multiconsult AS, Shell Technology Norway AS, Total E&P Norge AS, and project coordinator HSVA.

## REFERENCES

Hendrikse, H., 2017. *Ice-induced vibrations of vertically sided offshore structures*. PhD thesis, Delft University of Technology.

Hendrikse, H., and Nord, T. S., 2019. Dynamic response of an offshore structure interacting with an ice floe failing in crushing. *Marine Structures*, 65:271-290.

Hendrikse, H., Ziemer, G., and Owen, C. C., 2018. Experimental validation of a model for prediction of dynamic ice-structure interaction. *Cold Regions Science and Technology*, 151:345-358.

Hinse, P., Müller, F., and Ziemer, G., 2017. IVOS Progress Report: April 2017. Technical Report, 41p., HSVA, Hamburg.

Huang, Y., Shi, Q., and Song, A., 2007. Model test study of the interaction between ice and a compliant vertical narrow structure. *Cold Regions Science and Technology*, 49:151-160.

Jeong, S. and Baddour, N., 2010. Comparison of characteristic failure frequency models for ice induced vibrations. *JP Journal of Solids and Structures*, 4(3):115-137.

Kärnä, T., Andersen, H., Gürtner, A., Metrikine, A., Sodhi, D. S., Loo, M., Kuiper, G., Gibson, R., Fenz, D., Muggeridge, K., Wallenburg, C., Wu, J.-F., and Jefferies, M. G., 2013. Ice-induced vibrations of offshore structures - looking beyond ISO 19906. In *Proceedings of the 22nd International Conference on Port and Ocean Engineering under Arctic Conditions*, page 12, Helsinki, Finland.

Kärnä, T., Izumiyama, K., Yue, Q., Qu, Y., Guo, F., and Xu, N., 2007. An upper bound model for self-excited vibrations. In *Proceedings of the International Conference on Port and Ocean Engineering under Arctic Conditions*, Vol. 1, pages 177-189, Dalian, China.

Muhonen, A., 1996. *Evaluation of three ice-structure interaction models*. PhD thesis, Helsinki University of Technology.

Owen, C. C., 2017. *Ice-induced vibrations of vertically sided model structures: Comparison of structures with circular and rectangular cross-section subjected to the frequency lock in regime*. Master thesis, Delft University of Technology.

Owen, C. C., and Hendrikse, H., 2018. Ice-induced Vibrations of Model Structures with Various Dynamic Properties. In *Proceedings of the 24th IAHR International Symposium on Ice*, pages 376-385, Vladivostok, Russia.

Yap, K. T., and Palmer, A. C., 2013. A model test on ice-induced vibrations: structure response characteristics and scaling of the lock-in phenomenon. In *Proceedings of the 22nd International Conference on Port and Ocean Engineering under Arctic Conditions*, pages 1-11, Helsinki, Finland.

Ziemer, G., 2017. Research Project IVOS – Ice-induced Vibrations of Offshore Structures. Technical Report. http://dx.doi.org/10.13140/RG.2.2.34529.40801. (4p).

Ziemer, G., 2018. IVOS Interim Report: Model Tests Phase 3. Technical Report, 15p., HSVA, Hamburg.

Ziemer, G., and Hinse, P., 2017. Relation of maximum structural velocity and ice drift speed during frequency lock-in. In *Proceedings of the 24th International Conference on Port and Ocean Engineering under Arctic Conditions*, pages 1-12 (POAC17-071), Busan, Korea.